Rapid and Multifaceted Characterization of the Effects of the Secreted EVome in Pancreatic Cancer: A Global Omics Approach for Screening Putative Biomarkers

Harrys Kishore Charles Jacob (harryskcjacob@miami.edu)
University of Miami, Miller School of Medicine

Rossana Signorelli
University of Miami

John Lalith Charles Richard
University of California San Diego

Tyler Kashuv
University of Miami

Shweta Lavania
University of Miami, Miller School of Medicine

Ashley Middleton
University of Miami, Miller School of Medicine

Beatriz Aguilar Gomez
University of Miami, Miller School of Medicine

Anthony Ferrantella
University of Miami, Miller School of Medicine

Haleh Amirian
University of Miami, Miller School of Medicine

Junyi Tao
University of Miami, Miller School of Medicine

Aysha Burcu Ergonul
University of Miami

Melinda Minucci Boone
University of Miami

Marco Hadisurya
Purdue University

Weiguo Andy Tao
Purdue University

Anton Iluik
Tymora Analytical Operations

Monica Garcia-Buitrago
University of Miami, Miller School of Medicine
Rajinder Dawra
University of Miami, Miller School of Medicine
Ashok Kumar Saluja
University of Miami, Miller School of Medicine

Research Article

Keywords: Pancreatic cancer, extracellular vesicles, hybrid TMA, EVtrap, proteomics, tumor microenvironment, Sfrp2, Loxl2, Mmp3, Kif5b, pre-metastatic niche , microbiome, Hybrid TMA, omics

Posted Date: March 30th, 2022

DOI: https://doi.org/10.21203/rs.3.rs-1489466/v1

Abstract

Background: Pancreatic cancer is one of the most difficult cancers to detect early and most patients die from complications arising due to distant organ metastases. The lack of bona fide biomarkers is one of the primary reasons for the late diagnosis of this cancer. Most researchers have focused on screening strategies to characterize biomarkers that show promise in preclinical models but eventually fail in a clinical scenario. Pancreatic cancer is a multifactorial disease and warrants a multi-omics approach to identify novel biomarkers for early diagnosis.

Methods: In order to characterize the proteome, Extracellular vesicles (EVs) isolated from different *in vitro* conditions mimicking interactions between pancreatic cancer epithelial and stromal cells were isolated and subjected to high throughput mass spectrometry. Biological activity of the secreted EVome was analyzed by investigating changes in distant organ metastases and early changes in the microbiome. Putative biomarkers were selected and validated using a mouse-human hybrid TMA that was specifically generated for this study. As potential targets, immunohistochemical analysis of protein candidates (Kif5b, Sfpr2, Loxl2, and Mmp3) was performed on the TMA to assess their potential as candidates for early discovery of pancreatic cancer.

Results: The EVome of epithelial and stromal cells co-cultured with each other is distinctly different from individual cells with distinct protein compositions. While these proteomes could not induce significant changes in Pre-Metastatic Niche (PMN) modulation and distant organ metastases, they did induce significant early changes in the microbiome, as indicated by changes in the α and β-diversities in experimental animal models. Novel biomarkers validated in this study, such as Kif5b and Sfrp2 show promise for early detection and investigation of pancreatic cancer.

Conclusions: Multi-omics analyses of EVs from mimicking conditions of tumor stromal interactions resulted in the identification of Kif5b and Sfrp2 as bona fide biomarkers with biological activity which could prove to be immensely helpful in improving early detection and diagnosis of pancreatic cancer.

1. Background

Pancreatic Ductal Adenocarcinoma (PDAC) is a highly aggressive cancer with a survival rate of less than 11% and is expected to become the second leading cause of cancer-related deaths [1]. The poor prognosis is primarily due to the presentation of patients with locally advanced tumors at the primary site or inoperable distant organ metastases. Currently, there is a lack of biomarkers to identify pancreatic cancers in relatively early pathological stages primarily due to lack of data on early changes in cancer development. Carbohydrate antigen 19 – 9 (CA19-9) is currently the most effective biomarker for pancreatic cancer [2, 3] with a median diagnostic sensitivity of 79% and a median specificity of 80%, which limits its use in the screening of pancreatic cancer [4]. Valdidation of biomarkers in a clinical setting is challenging and there is a constant need to develop or revise newer staging systems with several circulating biomarkers before being accepted in clinical settings [5–8].

Here, we wanted to develop a pipeline to investigate rapidly the potential of biologically significant biomarkers using a multiple “omics” based approach. To this end, our aim was to identify a biological component that is seen as a major regulator of communication between cancer cells and other cell types seen in pancreatic cancer. Hence, we focused on investigating the role of extracellular vesicles (EVs), which are secreted from normal as well as diseased (cancer) cells and are known to play a significant role in pancreatic cancer signaling [9–11]. EVs are particles that range anywhere from 30 to 500 nm in diameter and have a lipid bilayer encapsulating lipids, proteins, and nucleic acids. Exosomes are a smaller subset of EVs ranging from 30–200 nm and have been implicated in pancreatic cancer cell proliferation, metastasis, EMT, and angiogenesis [12]. EV cargo has been implicated in either increasing [13] or decreasing [14] tumor cell proliferation in the pancreas and is a vital source for biomarkers. Though all cells release EVs, the sub- populations of EVs secreted from the cancer cells interact and communicate with the immediate tumor microenvironment (TME) and the associated circulatory system, thereby, making them excellent candidates for studying the early stages of the cancer even before the manifestation of symptoms [15]

The role of the tumor microenvironment (TME) in cancer development has been a field of intense research over the last few decades. Pancreatic TME is characterized by a dense stromal component, immune cells, neoplastic cells, cancer stem cells, and cancer-associated fibroblasts. Acellular components, including the Extracellular matrix (ECM), cytokines, growth factors, and secreted ligands resulting in intricate signaling pathways contribute to the complexity of the TME [16]. Naïve stromal or Pancreatic stellate cells (PSCs) are activated by cancer cells to induce fibrosis thus creating a physical barrier around the tumor cells which results in poor vascularization, poor immune cell infiltration. [17–19]. This desmoplastic stroma is a characteristic hallmark of Pancreatic Ductal AdenoCarcinoma (PDAC) in, both the primary and metastatic sites and limits the accessibility to chemotherapy [20]. In our study, we hypothesize that the EVs play a key role in mediating the interaction between pancreatic cancer cells and the TME, eventually resulting in the establishment of a desmoplastic environment which prevents the delivery of effective chemotherapeutic strategies. Thus, investigating changes in the EV populations secreted by the cells within the TME could be immensely useful for detection of early biomarkers for diagnosis in pancreatic cancer. We chose to focus on EVs secreted by the interaction between cancer cells and PSCs in the TME. Cell motility, cell adhesion, and the proliferative index of cancer cells have been known to be modulated by secreted EVs by affecting ECM proteins such as fibronectin [21]. Previously published study from our group has also shown that PDAC circulating tumor cells (CTCs) secrete EVs that can modulate neutrophil granulation modifying the immediate microenvironment [22] thus, providing impetus for the investigation of thes secreted EVome that is generation by tumor and stromal cell interaction in the TME.

PDAC is an extremely aggressive disease with high metastatic potential which explains the meager 5-year survival rate among patients (only 3%) [23]. Pioneering work has shown that exosomes (which are a smaller subset of EVs) derived from pancreatic cancer cell lines induce liver pre-metastatic niche (PMN) formation in naive mice and increase liver metastatic burden [24]. In recent years, there have also been several studies that show a variety of microorganisms colonized in pancreatic cancer tissues which are

now known to be involved in the development of pancreatic cancer regulating inflammation, metabolism, immune changes, and tumor microenvironment changes [25]. In colon cancer, there is an interplay between changes in the genome, metabolome, and the microbiome to effect changes in tumor development and metastasis [26, 27]. Here, we show that the cancer cell EVome does induce significant changes in the microbiome of experimental mice. Additionally, on assessing the expression of candidate proteins in mouse-human hybrid TMAs, out of may candidates analyzed, we identified Kif5b and Sfrp2 to be potential early markers for TME remodeling in pancreatic cancer.

2. Methods

2.1 Mouse derived cell lines

KPC cancer cells were isolated from a 5-month-old LSL-Kras^{G12D}/LSL-Trp53^{R172H}/Pdx1Cre GEMM. Flow cytometric enrichment of Cd326^{+}/Cd31^{-}/Fsp1^{-}/Cd45^{-} cells was performed. The positively enriched cells were cultured in DMEM-F12 medium with 10% FBS. PSCs were isolated according to protocols described earlier [28]. Isolated PSCs were cultured in IMDM with 20% FBS. Cells were cultured in FBS containing media and shifted to medium containing exosome depleted FBS prior to the experiment. 10^8 cells were taken in each condition for the KPC cells alone or the PSC cells alone while for the co-culture condition, 9 times the number of PSCs were taken compared to the KPC cells mimicking conditions that are seen *in vivo.* Cells were maintained in the exosome-depleted FBS containing media for 24 hours and the supernatant was collected and concentrated using a 10KDa filter.

2.2 EV Isolation

One hundred ml of cell culture supernatant from all the three cell lines was collected and concentrated using a 10kDa filter. Ten ml of the concentrate was incubated with magnetic EVtrap beads (Tymora Analytical Operations). The samples were incubated by shaking or end-over-end rotation for 60 minutes according to the manufacturer's instructions [29]. The supernatant was removed using a magnetic separator rack, the beads were washed once with PBS, and the EVs were eluted by two 10 minute incubations with 100mM of fresh trimethylamine (TEA, Millipore Sigma). Simultaneously, a fraction of the concentrated supernatant was also subjected to Transmission Electron Microscopy (TEM) and western blot analysis of EV markers.

2.3 Flow cytometric characterization of EVs

The Exo-Flo capture kit was used to characterize the classical markers expressed on the surface of EVs after they were concentrated. Cd63, Cd81, and Cd9 biotin capture antibodies (SBI Bioscience Cat# EXOFLOW150A-1) and antiHsp70 biotin-conjugated (Enzo Lifesciences Cat# ADI-SPA-815B-F) were first coupled with magnetic streptavidin beads and were incubated with 1 ml of EVs isolated after concentration. A PBS wash step was done to remove unbound EVs or other contaminants. The cells were stained with ExoFITC (excitation and emission wavelengths of 494nm and 518nm) and subjected to flow

cytometry. The samples were acquired on a Beckman Coulter CytoFlex S and CytExpert 2.3 was used for acquisition of data. EVs isolated from PanCO2 cell line were used as a published control [30].

2.4 Transmission Electron Microscopy (TEM)

EVs were resuspended in 2% paraformaldehyde and loaded on carbon Formvar-coated copper grids, which were subsequently stained with uranyl acetate. The EVs were fixed overnight in 2% glutaraldehyde in 0.1M phosphate buffer, post-fixed for 1 hour in 2% osmium tetroxide in 0.1M phosphate buffer, dehydrated through a series of graded ethanols, and embedded in EM-bed (Electron Microscopy Sciences, Fort Washington PA). The glass coverslip was dissolved in hydrofluoric acid. 100 nm sections were cut on a Leica Ultracut EM UC7 ultramicrotome and stained with uranyl acetate and lead citrate. The grids were viewed at 80 kV in a JEOL JEM-1400 transmission electron microscope and images captured by an AMT BioSprint 12 digital camera.

2.5 Preparation of Samples for LC-MS

The isolated and dried EV samples were lysed to extract proteins using the phase-transfer surfactant (PTS) aided procedure [29]. The proteins were reduced and alkylated by incubation in 10 mM TCEP and 40 mM CAA for 10 min at 95°C. The samples were diluted fivefold with 50 mM triethylammonium bicarbonate and digested with Lys-C (Wako) at 1:100 (wt/wt) enzyme-to-protein ratio for 3 h at 37°C. Trypsin was added to a final 1:50 (wt/wt) enzyme-to-protein ratio for overnight digestion at 37°C. To remove the PTS surfactants from the samples, the samples were acidified with trifluoroacetic acid (TFA) to a final concentration of 1% TFA, and ethyl acetate solution was added at 1:1 ratio. The mixture was vortexed for 2 min and then centrifuged at 16,000 × g for 2 min to obtain aqueous and organic phases. The organic phase (top layer) was discarded and the aqueous phase was collected. This step was repeated once more. The samples were dried in a vacuum centrifuge and desalted using Top-Tip C18 tips (Glygen) according to manufacturer's instructions. A portion of each sample was used to determine peptide concentration with Pierce Quantitative Colorimetric Peptide Assay, and all samples were normalized based on total peptide amount. The samples were dried completely in a vacuum centrifuge and the majority of each sample was used for phosphopeptide enrichment using PolyMAC Phosphopeptide Enrichment Kit (Tymora Analytical) according to the manufacturer's instructions. About 1% of each normalized sample was also injected directly in the LC-MS for proteomics analysis.

2.6 LC-MS/MS Analysis

Dried peptide and phosphopeptide samples were dissolved in 4.8 µL of 0.25% formic acid with 3% (vol/vol) acetonitrile and 4 µL of each were injected into an EasynLC 1000 (Thermo Fisher Scientific). Peptides were separated on a 45-cm in-house packed column (360 µm OD×75 µm ID) containing C18 resin (2.2 µm, 100 Å; Michrom Bioresources). The mobile phase buffer consisted of 0.1% formic acid in ultrapure water (buffer A) with an eluting buffer of 0.1% formic acid in 80% (vol/vol) acetonitrile (buffer B) run with a linear 60- or 90-min gradient of 6–30% buffer B at flow rate of 250 nL/min. The Easy-nLC 1000 was coupled online with a hybrid high-resolution LTQ-Orbitrap Velos Pro mass spectrometer (Thermo Fisher Scientific). The mass spectrometer was operated in the data-dependent mode, in which a

full-scan MS (from m/z 300 to 1,500 with the resolution of 30,000 at m/z 400), followed by MS/MS of the 10 most intense ions [normalized collision energy – 30%; automatic gain control (AGC) – 3E4, maximum injection time – 100 ms; 90sec exclusion].

2.7 Maxquant Label Free quantitation

MS raw files were analyzed using the MaxQuant software [31]. Peptides were searched against the human Uniprot FASTA database using the Andromeda search engine [32], integrated into MaxQuant. Oxidation and N-terminal acetylation, P/T/S phosphorylations were set as variable modifications, while carbamidomethyl was fixed. Trypsin was chosen as the digestion enzyme with a maximum of 2 missed cleavages. Identified peptides had an initial precursor mass deviation of up to 6 ppm and a fragment mass deviation of 0.6 Da. The false discovery rate (FDR) for peptides (minimum of 7 amino acids) and proteins was 1%. A reverse sequence database was used in determining the FDR. For label-free protein quantification, only unique peptides were considered. A contaminant database provided by the Andromeda search engine was used. All proteins matching the reverse database or labeled as contaminants were filtered out. Label-free protein quantification (LFQ) values were obtained through MaxQuant quantitative label-free analysis [31].

2.8 Data Analysis

The abundances of proteins from each group were log (2) transformed and grouped into 3 distinct categories: KPC (cancer cells), PSC (stellate cells), and CoC (co-culture condition). The proteins with detected abundances in at least one category in any condition were taken for analysis. The imputation for the missing abundances was performed by assigning small random values from the normal distribution to each missing value (width = 0.3, down shift = 1.8). Missing values were normally caused by very low abundances. All abundances for each protein were normalized by using width-adjustment. The first, second and third quartile (q1, q2, q3) were calculated from the distribution of all values. The second quartile (which is the median) was subtracted from each value to center the distribution and divided by the width in an asymmetric way. All values that were positive after subtraction of the median were divided by q3 - q2 while all negative values were divided by q2 - q1 following which an ANOVA test was performed. Only those proteins with q-value (FDR) less than 0.05 were used in the heatmap. All enrichment analyses with the gene lists were done on GorillaGO [33], an intuitive graphical web application to visualize pathways from different databases. Only pathways that had a p-value of ≤ 0.05 were considered. The Reactome [34] database was used for all pathway analyses. All non-human identifiers were converted to their human equivalents and IntAct interactors were selected to increase the analysis background.

2.9 EV Education and measurement of tumor burden in orthotopic implant models

Five µg of EVs were injected into the retro-orbital venous sinus of naïve 6–8 week C57BL6 mice. The injections were done every other day for a period of 25 days. Post education, 500000 KPC cells were injected orthotopically in growth factor reduced Matrigel (Corning Cat# 354230). Saline was injected into

the control mice. The mice were sacrificed 3 weeks post-surgery and the liver weights were measured and compared to control mice. All mice were monitored according to IACUC guidelines and sacrificed if excessive deterioration in health was observed. The mice were fed ad-libitum.

2.10 Microbiome Analyses

2.10.1 Fecal Collection

Pellets of fecal matter were collected from five individual mice from each group at time point 0 before injection and at time points two weeks after education. Stool samples were collected in RNase/DNase-free tubes (Catalog #: C-2170, Denville Scientific, Holliston, MA, USA) and were immediately frozen on dry ice and then stored at − 80°C; PowerSoil DNA isolation kit (Qiagen Cat #47016) was used to extract genomic DNA and was stored at -80°C until amplification. DNA was isolated using DNeasy 96 PowerSoil Pro QIAcube HT Kit with QIAcube HT liquid-handling machine (Qiagen, Maryland, USA).

2.10.2 Quantitative real-time PCR amplification for Illumina sequencing

The 16S sequencing was performed at the University of Minnesota Genomic Center [35]. 25ug of DNA was used as templates for PCR amplification of the V4 region of the 16S rRNA gene. Degenerate primer sets were designed with Illumina index sequences on the 5' end of the reverse primer, which were specific to each fecal DNA sample and allowed for multiplex sequencing. Primers also contained Illumina PCR primer sequences (reverse primer) and Illumina TruSeq Universal Adapter sequences (forward primers) for library creation. The primer sequences (16S-specific portion in bold) used were Meta_V4_515F (TCGTCGGCAGCGTCAGATGTGTATAAGAGACAGGTGCCAGCMGCCGCGGTAA) and Meta_V4_806R (GTCTCGTGGGCTCGGAGATGTGTATAAGAGACAGGGACTACHVGGGTWTCTAAT). The indexing primers are as follows: This step adds both the index and the flow cell adapters. [i5] and [i7] refer to the index sequence codes used by Illumina. The p5 and p7 flow cell adapters are in bold. Forward indexing primer: ATGATACGGCGACCACCGGATCTACAC[i5]TCGTCGGCAGCGTC; Reverse indexing primer: CAAGCAGAAGACGGCATACGAGAT[i7]GTCTCGTGGGCTCGG. PCR reactions were performed using KAPA HiFidelity Hot Start Polymerase. PCR 1 (using the Meta_V4_515F/Meta_V4_806R primer pair): 95°C 5 minutes, 20 cycles (98°C 20 seconds, 55°C 15 seconds, 72°C 1 minute), followed by holding at 4°C. After the first round of amplification, PCR 1 products were diluted 1:100 and 5 µl of 1:100 PCR 1 was used in the second PCR reaction. PCR 2 (using different combinations of forward and reverse indexing primers): 95°C 5 minutes, 10 cycles (98°C 20 seconds, 55°C 15 seconds, 72°C 1 minute), followed by holding at 4°C.

2.10.3 DNA sequencing

Genomic DNA sequencing was performed using Illumina MiSeq at the University of Minnesota Genomic Center (UMGC). Pooled, size-selected samples were denatured with NaOH, diluted to 8 pM in Illumina's HT1 buffer, spiked with 15% PhiX, and heat-denatured at 96°C for 2 minutes immediately prior to loading. The MiSeq 600 cycle v3 kit was used to sequence the sample. Nextera adapter sequences for post-run

trimming were as follows: Read 1: CTGTCTCTTATACACATCTCCGAGCCCACGAGACNNNNNNNNATCTCGTATGCCGTCTTCTGCTTG Read 2: CTGTCTCTTATACACATCTGACGCTGCCGACGANNNNNNNNGTGTAGATCTCGGTGGTCGCCGTATCATT.

2.10.4 Sequence processing and analysis

Demultiplexed sequence reads were clustered into amplicon sequence variants (ASVs) with the DADA2 package (version 1.21.0) (27214047) implemented in R (version 4.0.3) and RStudio (version 1.1.463). The steps of the DADA2 pipeline include error-filtering, trimming, learning of error rates, denoising, merging of paired reads, and removal of chimeras. The ASV table generated by DADA2 was imported into the QIIME2 pipeline [36] for diversity analyses and taxonomic assignment. Diversity analyses were performed by using the Qiime diversity core-metrics-phylogenetic script with sampling depth of 50,000. Taxonomic assignment of ASVs was done to the genus level using a naïve Bayesian classifier (29773078) implemented in QIIME2 with Greengenes reference database (13_8 99%) (22134646). LDA Effect Size (LEfSe) (21702898) was generated by uploading the taxonomic assignment table to the galaxy app (https://huttenhower.sph.harvard.edu/galaxy/) to detect differentially abundant taxa across groups. The threshold on the logarithmic LDA score for discriminative features was set to 2. Kruskal-Wallis test was used to detect if α diversity differed across treatments. Permutational multivariate analysis of variance (PERMANOVA) was used to detect if β diversity differed across treatments. Benjamini-Hochberg method was used for controlling false discovery rate (q-value). Bar plot and heat map were generated using microbiomeanalyst (https://www.microbiomeanalyst.ca/) [37].

2.11 Generation of a Mouse-Human Hybrid TMA

A mouse and human- specific TMA was generated for the rapid validation of biomarkers that would need to be assayed. A majority of the samples were taken from the KPC model of pancreatic cancer which is one of the most widely used models for disease modeling [38]. Cores were taken from KPC mice pancreas at various stages of development. Samples were taken from both diseased pancreas and adjacent non-neoplastic areas as well as from normal pancreas. Distant organ mets to lungs, liver or spleen were also cored onto the TMA. Representative sample cores were also taken from subcutaneous tumor models, their associated metastases, and from subcutaneous models of circulating or dissociated tumor cells. Diseased human pancreas along with normal samples were also taken for assesment in clinic. Control cores of heart and colon tissue were taken for orientation purposes and to assess staining in other organs. Cores were also taken from an inducible Kras model that was generated by subcutaneously implanting the cells in normal mice. 1mm cores were taken from pathologically verified and arrayed into a TMA with multiple duplicate cores in different locations. The detailed TMA map of all sections arrayed on the hybrid mouse-human TMA is shown in **Supplementary File S5.**

2.12 Histochemical validation of selected markers.

The following antibodies were used for histochemical validation anti Loxl2 (Thermo Cat# PA5-85210; 1:500 dilution), anti Mmp3 (Thermo Cat# 17873-1-AP; 1:500 dilution), anti Sfrp2 (Thermo Cat# PA5-76794; 1:250 dilution) and anti Kif5b (Abcam Cat# ab167429; 1:500 dilution). The TMA cores were heated at 60°C overnight and then hydrated conventionally, following which antigen retrieval was done by steaming the slides for 20 minutes in Antigen unmasking solution Tris Based (VectorLabs Cat#H3301-250), following which slides were cooled to room temperature. Endogenous peroxidase, pseudoperoxidase and alkaline phosphatase in FFPE sections were blocked with Bloxall (VectorsLabs Cat # SP6000-100) for 10 minutes. Cells were then washed in IHC wash buffer (PBS with 0.1% Tween20) for 5 minutes following which they were incubated with normal goat serum (2.5%) for 20 minutes. The antibodies were then diluted in goat serum at the dilutions mentioned earlier and the sections were incubated at 4°C overnight. The slides were then washed in wash buffer for 5 minutes and incubated for 30 minutes with ImmPRESS Universal Polymer Reagent (VectorLabs Cat# MP-7451) for 30 minutes. The slides were washed twice in wash buffer and incubated with ImmPACT DAB EqV peroxidase substrate solution (VectorLabs Cat#SK4103-400) for 5 minutes. Slides were then washed in wash buffer twice for 5 minutes each and then rinsed in tap water. The slides were counterstained with Hematoxylin QS counterstain (VectorLabs Cat# H3404-100) for 60 seconds and rinsed in tap water. The slides were dehydrated conventionally and then mounted with Vectamount permanent mounting medium (VectorLabs Cat# H5000-60). The slides were checked and scored by an expert Pathologist (G-B.M.).

3. Results

3.1 Characterization of EVs secreted from individual cells and co-culture conditions

Cancer epithelial cells were isolated from a 5-month-old KPC mouse with pancreatic tumors. The cells were sorted to obtain a heterogeneous population of cancer cells that were positive for Epcam and negative for Cd45, Cd31, and Fsp1. This would help ensure a pure population of cancer epithelial cells. We excluded fibroblast, endothelial cells, and cells of any hematopoietic origin. A heterogeneous population of cells was isolated after sorting and cultured for four passages. Naïve stromal cells were obtained from C57BL6 mice as previously described by Apte et al [39]. In a pancreatic tumor setting, the ratio of cancer cells to stromal cells is around 1:9 and we decided to adapt the same co-culture conditions when the cancer cells designated as KPC cells were mixed with stromal cells designated as PSCs (Pancreatic Stellate Cells). KPC cells and PSCs were also cultured in isolation to identify secreted vesicles from the individual cell types. The cell culture supernatant was collected, concentrated, and subjected to transmission electron microscopy (TEM) and flow cytometric analysis to characterize the size and distribution of particles and to help assess purity of the samples. Transmission electron microscopy identified vesicles ranging from 20nm to greater than 500nm **[**Figure 1 **(i-iii)].** Additional fractionation was not done to separate vesicles of a particular size, as we wanted to investigate the wholesome contribution of all vesicles to TME remodeling. Conventional vesicles have high concentrations of tetraspanin proteins such as Cd63, Cd9, and Cd81, in addition to Hsp70 which is a

pancreatic cancer-specific marker that has also been reported in the exosomal or extravesicular population [40, 41]. A Panc02 line was used as the control pancreatic cell line that is known to secrete EVs [30, 42]. Flow cytometric quantification of EV markers was carried out **[**Figure 1 **(iv)].** The different cell types showed varying concentration of these assayed proteins **[**Figure 1 **(iv)].**

3.2 Mass spectrometric characterization of EVome shows a distinct proteome

In addition to conventional proteins characterized on the surface of the EVs, we wanted to investigate the proteome enclosed within these secreted particles. To accomplish this, we collected the supernatant from the different experimental conditions [KPC alone, PSC alone and Co-culture (CoC)]. All samples were processed in triplicate and the purified EVs were subjected to mass spectrometry analysis. Initial proteomic analyses of individual experimental conditions identified 721 proteins from the KPC cells, 400 proteins from the PSCs and 540 proteins from the co-culture condition. Of the identified proteins, 282 were unique to KPC cells, 65 to stellate and 267 in the co-culture condition indicative of the diversity of the different groups providing a milieu for the identification of candidate proteins that regulate or in turn, were regulated in the immediate two-cell tumor microenvironment. Phosphorylation patterns on proteins are indicative of signaling status and activity, hence, we looked at the phosphoproteome of the proteins that are secreted in each cell condition. We identified 489 phosphoproteins in the KPC cell line, 543 in the stellate cells, and 512 in the co-culture condition. Among the proteins, there were 250 phosphorylated proteins that were unique to the co-culture condition, 34 in the stellate PSCs and 130 in the KPC cell line. Venn distributions of proteins and phosphoproteins identified from this study indicate the variability and uniqueness of the EVome detected within the proteome and phosphoproteome datasets **[**Figure 1 **(v-vi)]**. The complete list of identifications from the proteomics and phosphoproteomics analyses are shown in **Supplementary File S1**.

Statistical analysis of the data was performed to identify variability among replicates to assess proteome data quality by comparing the relative protein quantification among the three biological replicates in each group. Identifications among the different triplicates of proteins **[**Figure 2**(i)]** presented as multiscatter plots with Pearson correlation values of 0.7 to 1, suggest a good correlation between data obtained from the KPC, PSC, and CoC (Co-culture) experimental conditions. Similarly, correlation values of 0.6-1 were observed among the triplicates of conditions when phosphoproteins were analyzed **[**Figure 2**(ii)]**. PCA plots of the LC-MS data demonstrated that the triplicates were closely clustered among the proteins **[**Figure 2**(iii)]** and phosphoproteins **[**Figure 2**(iv)]** as observed by the separation trends between the different conditions. To investigate trends among the candidate proteins and phosphoproteins identified in the study, an unsupervised hierarchical clustering was done. The replicates clustered with each other indicating good reproducibility within each condition. Additionally, we identified four clusters among the proteins indicative of different total protein expression trends **[**Figure 2**(v)]**. A more complex trend was observed among the phosphoproteins with five clusters **[**Figure 2**(vi)]**. Parallel coordinate plots for protein clusters identified in the study are shown in [**Supplementary Fig. 1(i)].** Parallel coordinate plots follow the expected trend across clusters, indicative of signature expression patterns within the proteins identified.

No observable trends were observed in the parallel coordinate plots for identified phosphoproteins and hence they were excluded for target selection **[Supplementary Fig. 1(ii)]**. Among the different clusters, Cluster 1 included several molecules that were downregulated in KPC EVs and were overexpressed in CoC and in PSCs. While in cluster 2, the majority of the molecules showed a trend of being overexpressed in the CoC EVs but not in the KPCs and PSCs. Cluster 3 identified the majority of proteins that were overexpressed in PSC and downregulated in KPC and CoC EVomes and finally, cluster 4 showed multiple molecules that were downregulated in CoC, in comparison to other conditions. The list of proteins that were identified and used in the downstream analyses along with cluster classification is shown in **Supplementary File S2**.

3.4 Gene Ontology (GO) analysis of the EVome identifies novel signaling elements

GO analysis of the proteins identified from KPC cells showed that they are mostly enriched for signaling receptor and protein binding molecular functions (actin, growth factor and enzyme); cellular response to organic substances, cytokines, and anatomical structure morphogenesis and development biological processes that are primarily extracellular, cell surface or ECM in their cellular component localizations. Extravesicular proteins from the stellate cells enrich for ECM structural molecules or involved in protein binding molecular functions (SMAD, growth factor, PDGF, and IGF). Common enriched biological processes include skin development, cell and biological adhesion, cellular response to stimulus, and collagen fibril organization. Most proteins were localized to a part of the ECM component or involved in collagen and fibrillar trimerization. It was interesting to note that 540 proteins identified from the co-culture condition enriched for biological processes that were a cellular response to an organic or chemical stimulus among other response pathways, biological functions involving SMAD, growth factor or PDGF binding for conferring tensile strength to the ECM. Similarity in cellular localization of proteins were observed in KPC and PSCs. Unique proteins identified in each group were subjected to Reactome analyses to get a better idea about the pathways that could be regulated. Significant pathways enriched in the KPC cells were association of TriC/CCT chaperonins, which target proteins during biosynthesis and related formation of tubulin folding intermediates, pre-folding mediated transfer of substrate to CCT/Tric, and proteins co-operating with β folding G-protein complexes. Top Reactome pathways enriched for the 65 unique proteins identified in the PSCs were pathways regulating striated muscle contraction, ARMS-mediated activation, defective PGM1, Factor XII, and SERPING1 casing hereditary angioedema, and in collagen degradation among others. The 267 unique proteins identified only in the co-culture conditions enriched for pathways regulating the assembly of collagen fibrils and other multimeric structures and involved in addition to being involved in post-translational protein phosphorylation, collagen biogenesis and degradation and ECM reorganization. The proteome that was identified in the three conditions are unique and contribute to distinct ECM remodeling capabilities. The detailed lists of all pathways enriched in the GO and Reactome analyses are provided in **Supplementary Files S3** and **S4**.

A Reactome analysis of the unique phosphoproteins identified in the KPC condition enriched for pathways that modulate heparin and heparan sulphate (HS-GAG) degradation and, interestingly, proteins

that regulate DNA synthesis on the laggings strand that are involved in Gap filling DNA repair or mismatch repair. Phosphoproteins identified in the stellate cells enriched for G2M/M DNA replication checkpoints and for proteins regulating amino acid transport across the plasma membrane and involved in Rhobtb1/2 GTPase cycle regulation. The 250 unique proteins identified in the co-culture condition were enriched for proteins that modulate post translational phosphorylation, and proteins regulating the Rhobtb GTPase cycle among other pathways. It is interesting to note that the phosphoproteins identified in all three conditions happen to modulate cell signaling and the GTPase cycle in pancreatic cancer, and regulate eukaryotic translation and initiation complexes, indicative of a much more specific role of the phosphoproteome. A list of the pathways enriched in all Reactome analyses is provided in **Supplementary File S4**.

3.5 EVs modulate the Pre-Metastatic Niche (PMN) to enhance metastatic burden in the liver

An experimental model of orthotopic splenic injection of KPC cells was used to determine whether there is an increase in the metastasis to the liver. Naïve 6–8 week old C57BL6 mice were retro-orbitally injected with 5µg of EVs to "educate" [24] and generate a PMN in the liver. EVs from KPC, PSC, and the CoC conditions were injected into mice for a period of 25 days. An additional condition was also included in the experiment that consisted of KPC and PSC derived EVs mixed in a 1:9 ratio to examine if a pool of individual cellular EVs can mimic CoC conditions. This would provide information on whether EVs secreted by *in vitro* conditions separately were sufficient to induce an increase in tumor metastasis or a unique population of EVs was being generated that could modulate metastasis only when the cells interact with each other. After the education period, KPC cells were orthotopically implanted into the spleen of the mice and the tumors were allowed to develop for a period of 3 weeks, following which the mice were sacrificed. Tumor weights of the liver were compared with control mice. A schematic of the experimental design in shown in Fig. 3 **(i)**. In comparison to wild-type mice, the treated mice all showed a substantial increase in the weight of the livers but did not show any significant difference within the different groups [Figure 3 **(ii)**]. The experiment was repeated several times with no statistically significant observation between groups injected with EVs from KPCs, stellate cells, or the co-culture conditions. A distribution of liver weight is shown in Fig. 3 **(iii)**, indicating no significant trend or change.

3.6 EVs induce early microbiome changes in a mouse model of metastasis

To investigate early changes in the gut microbiome of mice that were educated with EVs from different experimental conditions, fecal pellets were collected from mice at the end of two weeks of education. Fecal samples were collected from five mice in each group and DNA was isolated and subjected to microbiome enrichment and analysis. To investigate the differences between microbial communities from the different experimental conditions, β diversity was measured using weighted UniFrac distances and visualized with principal-coordinate analysis (PCoA) plots [Figure 4 **(i)**]. We observed that the different groups clustered apart, indicating unique bacterial enrichment in each of the experimental

groups and providing additional evidence that the EVs from different groups have a unique influence on the microbiome. Statistical analysis demonstrated that the distinct groups i.e., PBS, KPC, PSC, and CoC are significantly different from each other. The differences are statistically significant, with a measured q value of < 0.05 for all groups. When the intra-sample differences (α diversity) were measured by Faith's phylogenetic diversity, the co-culture microbiome diversity level was significantly lower than that of the other microbiomes (P < 0.05) **[**Figure 4 **(ii)]**. There were no statistically significant differences between the other groups. It is interesting to note EVs from each of the culture conditions, are selectively poised to induce changes in the mouse microbiome. LefSe (Linear Discriminant Analysis (LDA) analysis was additionally performed between the experimental samples to determine the bacterial taxa that were differentially enriched upon education with different types of EVs. Compared to the PBS control injections, bacteria from family *coriobacteriaceae*, genus *Adlercreutzia*, were enriched under PSC EV education. In the group educated with EVs from KPC cells, bacteria from the phylum *Tenericutes*, family *Mogibacteriaceae*, genus *Adlercreutzia*, were highly abundant, and bacteria from phylum *Firmicutes*, genus *coprococcus*, were more abundant in co-culture educated samples [Figure 4 **(iii)**]. Representative bar plots and heat maps of relative abundances at the phylum level are shown in Figs. 4 **(iv and v)**. Consistent with the analysis, phylum *Tenericutes* (orange bar) were more abundant in KPC condition. Similarly, phylum *Firmicutes* being the most abundant than other groups confirmed that it was enriched under co-culture condition.

3.7 Immunohistochemical validation of biomarkers identifies novel early biomarkers in pancreatic cancer

We investigated the contribution of EVs either from cancer cells or stellate cells in isolation and finally in a co-culture condition. The co-culture condition would be identical to *in vivo* models of PDAC where cancer cells interact with stromal cells to generate desmoplastic reaction and cancer progression. The strategy was to investigate if early changes observed in the EV population of cells could help predict and identify novel markers of TME remodeling. Thus, we picked protein candidates that are overexpressed in the co-culture conditions but are relatively low or downregulated in the KPC and normal stellate conditions alone. This could be attributed to molecules that are specifically modulated when cancer cells interact with stromal cells. The Cluster with most such molecules was Cluster 2 from the proteins list in **Supplementary File S6**. A heatmap of protein markers specifically observed in Cluster 2 is shown in **Supplementary Fig. 2.** We identified several markers that have been previously reported in literature to be involved in TME remodeling, such as Fibronectin, Cxcl2, Cxcl1, and Ccl7. A hybrid TMA was generated using mouse and human normal and diseased pancreas, metastases, KPC GEMM mice organs at different stages, subcutaneous and orthotopic models of pancreatic cancer and tumors and metastases from the EV education experiment described earlier. The hybrid TMA was generated after review from an expert pathologist, and it was arrayed in a format such that there were multiple representations across the slide. Due to the limitations imposed by the availability of antibodies that were reactive to both mouse and human samples, the following biomarkers Kif5b, Sfrp2, Loxl2, and Mmp3 were selected for validation. Representative images of tissue sections from mouse and human normal and diseased pancreas were stained by a histological stain Masson's Trichrome to verify histomorphological

differences. Additional staining on subsequent sections for Kif5b, Sfrp2, Loxl2 and Mmp3 was conducted to investigate differences in staining patterns in normal and diseased mouse and human tissue (Fig. 5).

3.7.1 Lysyl Oxidase Homolog 2 (Loxl2)

The LOXL family is composed of 5 protein isoforms (LOX and LOXL1-4) that are synthesized as inactive protoenzymes into the extracellular environment and subsequently cleaved into their active form [43], however, our analysis was only focused on the Loxl2 isoform.

Loxl2 showed strong expression in the normal pancreatic acini while expression was low in pancreatic ducts and negative in stroma. Staining in the diseased pancreas sections showed moderate expression in the murine tumor and stroma, while the human pancreas showed low to moderate expression in the tumor and low expression in the stroma (Figs. 5 and 6). Hepatocytes and pneumocytes stained weakly or were negative for Loxl2 expression. Lung, liver and axillary metastases showed higher expression of Loxl2 in the tumor cells. While no stroma was visible around the lung and axillary metastases, the stroma in the liver mets showed weak staining. Loxl2 expression is also high in metastases observed in mice and human samples. Moreover, it is strongly indicative of the diseased stroma to have been influenced by the cancer cells to secrete EV, which could possibly increase the level of expression in the adjacent stroma (Fig. 7). As for the KPC GEMM mice at different time points, the tumor stained strongly at 25 days, 3, and 7 months, indicating that Loxl2 was expressed early in the KPC models, thereby establishing it as an excellent marker for early diagnosis of PDAC in mice **(Supplementary Fig. 3)**. It is also interesting to note that there were distinct differences in the stromal staining where in the same section with diseased and adjacent normal tissue, the stroma around the neoplasia stained strongly for the marker while that around the adjacent normal did not, indicative of highly specific stromal effect in both mouse and human samples (Fig. 7). This indicates that the expression is an outcome of direct exposure of cancer cells to the stroma and is a much-minimized local effect. In terms of consistency in staining across the samples, the staining patterns were not consistent in most cases thereby limiting its utility as a suitable marker for further diagnostic purposes. Circulating and dissociated tumor cells isolated from KPC GEMM mice that were grown subcutaneously were strongly positive for Loxl2 indicating that the cancer cells in circulation also have high expression of the protein **(Supplementary Fig. 4)**.

3.7.2 Kinesin-1 Heavy chain (Kif5b)

The KIF1B gene codes for kinesin family member 1B, which is part of the kinesin family of proteins. In neurons, these proteins are responsible for transporting small, sac-like structures called synaptic vesicles whereas in other cell types, these proteins carry the mitochondria. Interestingly, not much is known regarding its expression in the normal or diseased pancreas in either mouse or human samples.

Normal pancreatic acini and ducts stained strongly for Kif5b while the stroma in normal mice or human samples stained weakly (Figs. 5 and 6). Hepatocytes did not or weakly stained while the hepatic ducts showed high expression. The lung alveoli and bronchi also showed overexpression in normal conditions. In the murine pancreas, the protein was highly expressed in both tumor and stroma, while in the human

pancreas, the protein expression was low to high in the tumor and low to negative in the stroma (Figs. 5 and 6). Lung, liver, and axillary metastases showed strong positivity in the tumor cells while the stroma in liver mets was weakly stained (Fig. 7). As for the KPC GEMM mice at different ages, the tumor and stroma were strongly positive for expression of Kif5b at 25 days, 3, and 7 months. As observed earlier with Loxl2, Kif5b staining in cancer cells and immediate stroma showed a strong positivity while in the normal pancreas, the acini were strongly positive but adjacent stroma was weakly positive for protein expression (Fig. 6). Strong staining was also observed in CTCs and DTCs cultured subcutaneously that were isolated from KPC GEMM mice indicative of it, possibly being a cancer cell secreted factor. Kif5b staining was highly consistent across sample types both for mouse and human and was assayed to be the strongest staining marker among all the markers assayed in our study. Thus, there is a distinct possibility that Kif5b could potentially be a viable and novel marker worthy of being investigated in pancreatic cancer.

3.7.3 Matrix Metalloprotease 3 (Mmp3)

Matrix Metallopeptidase 3, or MMP3, is a protein coding gene; MMP3 protein is identified in exosomes derived from mesenchymal stem cells [44] and is expressed in human bronchoalveolar fluid as well as plasma [45]. Proteins belonging to the MMP family are involved in the breakdown of the extracellular matrix in embryonic development, reproduction, tissue remodeling, as well as in metastasis.

On evaluation of staining on the hybrid TMA, normal pancreatic acini stained strongly while pancreatic duct weakly stained, and the stroma was negative for Mmp3. Hepatic ducts stained strongly while the hepatocytes were weak or negative for Mmp3. In the lung, alveoli stained weakly while the bronchi were strongly positive for the protein. Mmp3 had low expression in both tumor and stroma in murine and human pancreas (Figs. 5 and 6). Low expression was observed in the lung, liver, and axillary metastases as well (Fig. 7). The KPC GEMMs at different ages also showed weak staining. Interestingly, the only trend that was significantly consistent was the strong stromal staining in diseased pancreas; even though acini had strong staining in the normal pancreas, the surrounding stroma was negative for Mmp3 **(Supplementary Fig. 3)**. Mmp3 staining was comparatively weak with respect to all the stains except in the distant metastases (Fig. 7). The pattern of diseased stroma staining more positively than stroma surrounding normal acini was also observed in the hybrid TMAs for both mouse and human tissue (Fig. 6). Weak staining was also observed in both the DTC and CTC subcutaneous implants **(Supplementary Fig. 4)**. To summarize, our results indicate that the Mmp3 was a weakly staining marker, and the staining pattern was not consistent across samples thereby limiting its diagnostic value as a marker for pancreatic cancer.

3.7.4 Secreted Frizzled-related protein 2 (Sfrp2)

Soluble frizzled-related proteins, functioning as modulators of Wnt signaling, have major roles to play in regulating the cell growth and differentiation in specific cell types. Specifically, Sfrp2 has a role to play in the retinal development and for myogenesis.

Normal mouse and human pancreatic acini and ducts stained strongly for Sfrp2 while the stroma was negative. Normal murine hepatocytes and hepatic ducts were also strongly positive, while the human hepatocytes and hepatic ducts stained weakly. Normal lung alveoli and bronchi stained strongly as well. In the pancreas, the murine tumor and stroma stained strongly while the human tumor staining was variable with weak staining pattern in stromal cells (Figs. 5 and 6). All lung, liver, and axillary metastases were strongly positive in the tumor cells while only stromal cells observed in the liver mets were strongly positive (Fig. 7). In the different ages of KPC GEMM mice, the tumor and stroma strained strongly in the early juvenile mice **(Supplementary Fig. 3)**. The pattern of diseased stroma staining more positively than stroma surrounding the normal acini was also observed in the hybrid TMAs for both mouse and human tissue (Fig. 6). Strong positive staining was also observed in the CTC and DTCs as well **(Supplementary Fig. 4)**. As with Kif5b, Sfrp2 showed a similar consistent staining pattern across different tissues in both the mouse and humans. Thus, our study shows its utility as a strongly staining marker which could be used for further diagnostic purposes.

4. Discussion

Our study is a unique attempt at identifying and investigating the role of early EV- related biomarkers that can be quickly adapted for use in the detection of early stage pancreatic cancer, a disease that is notorious for its propenisty to metastasize quickly with barely any symptoms in the initial stages.

EVs or exosomes have been identified as promising candidates for the identification of biomarkers given their robustness in circulation and in being resistant to degradation. Translating *in vitro* findings to preclinical studies and eventually for validation into the clinic has a high failure rate. For our studies, we adopted a novel strategy of developing a mouse-human hybrid TMA that can be easily used to test biological significance of biomarkers. The TMA was developed by taking different developmental stages of tumors in the KPC GEMM mouse model. Additionally, it included cancers and adjacent normal tissue as well. Clinical normal and diseased tissues were also cored onto the TMA. Bi-species reactive antibodies were used to investigate the presence of Loxl2, Mmp3, Kif5b and Sfrp2.

Lysyl oxidase related protein-1 (LOR-1) (currently termed LOXL2) promotes tumor fibrosis and tumor invasiveness by invading blood vessels, nerves, and muscles adjacent to tumors [46]. High concentrations of LOXL2 significantly correlated with increased tumor malignancy and cells of LOXL2-expressing tumors are surrounded by high concentrations of dense collagen fibers and contained many fibrotic foci. Additionally, LOXL2 has gained attention due to its critical role in tumor progression and metastatic potential in pancreatic cancer [47]. The protein mediates the crosstalk of cancer cells [48, 49] and fibroblasts [50, 51], driving EMT [52–56], and regulating ECM remodeling and crosslinking [57, 58]. Inhibition of expression reduces tumor volume and metastasis in PDAC pre-clinical trials [57]. Thus, LOXL2 seems to be the key communicator between tumor cells and the tumor microenvironment and is known to mediate ECM remodeling and CAF activation [59]. MMPs are involved in not only cancer initiation and progression, but also functional promotion of angiogenesis, invasion, metastasis, and avoidance of immune surveillance. MMPs are primarily produced by stromal cells in response to

paracrine cytokine signaling in the tumor environment. While analyzing the expression of MMP3 molecules in a large panel of human pancreatic adenocarcinomas, evidence of the involvement of this pathway in all stages of pancreatic cancer progression. Further evidence that pancreatic acinar cell MMP3 interacts with KRAS to initiate pre-malignant alterations in the surrounding stroma was found using transgenic mouse models. Selective MMP-activation occurs in the CAM secretome even when cultured cells have no exposure to cancer cells. Hence, this shows the possibility a cell-autonomous mechanism where CAMs, with increased selective MMP activation and production, can contribute to the remodeling of the cancer microenvironment [60]. SFRP2 secreted from aged fibroblasts augment angiogenesis and metastasis of melanoma cells contributing to tumor progression [61]. Secreted plasma levels of SFPP2 is a non-invasive tool for the detection of gastric cancer and is a valuable serum tumor marker [62]. It has been a fibroblast-secreted marker and in colorectal cancer, Sox2-dependent CAF population secrete Sfrp2 and inactivation of Sox2 or Sfrp1/2 in CAFs impairs the induction of migration and invasion of colon cancer cells, including their tumorigenicity in vivo [63]. In pancreatic cancer, SFRP2 cell-free DNA promoter hypermethylation in plasma is a biomarker for pancreatic adenocarcinoma [64]. In addition, the hypermethylation and aberrant expression of frizzled-related protein genes are common in pancreatic cancer and have been shown to be involved in pancreatic carcinogenesis[65]. TET1 protein binds to SFPR2 and inhibits canonical and non-canonical Wnt signaling pathways; this process prevents EMT transition in pancreatic tumors [66]. All biomarkers showed similar patterns of staining across mouse and human samples. Cancer cells strongly expressed these proteins in both primary and distant metastases. It is difficult to validate the presence of the protein in human samples in an age dependent manner due to lack of clinical samples. In KPC GEMM mice, the expression of Kif5b, Sfrp2, and Loxl2 was high in mice as old as 35 days. Mmp3 however, stained weakly, thereby forcing us to disregard it as a putative early biomarker. Thus, our study provides compelling evidence for the utility of Sfrp2 and Kif5b as putative markers for early pancreatic cancer diagnosis.

Additionally, our experimental findings suggest that the secreted EVs contain several hundred signaling moieties that can modulate the TME. Studies by several groups have shown that exosomes secreted from cancer cells can modulate the pre metastatic niche and influence tumor metastases in a liver metastasis animal model of pancreatic cancer [24]. If TME remodulation is different, we hypothesized that the rate of metastases would also be different. To test this assertion, we injected EVs that were purified from different experimental conditions such as those obtained from KPC cells, stellate cells and the cancer cells and stellate cells cultured together. There was no significant change in the liver weights or increase in the levels of metastasis in comparison to the control. This could partly be explained by our experimental setup. Short exposure times of 24 hours would not induce potent changes in the proteome to increase metastasis in the co-culture condition. However, the experimental limitation is that *in vitro*, cancer cells soon outnumber stellate cells even though they are nine-fold more abundant. Cancer cells are more aggressive and have rapid doubling times in comparison to stellate cells. The TME is composed of multiple cell types and other acellular factors such as cytokines and chemokines. By including additional cell types in the co-culture condition, we could have seen a more aggressive metastatic phenotype resulting in significant increase in liver metastasis. The development of an aggressive PMN was not

visible. It was imperative to investigate if the EVs that were injected into the mice could influence any biological activity. Several studies [67–70] have shown that there is a distinct pancreatic microbiome which could decisively influence the development of pancreatic cancer. To investigate this phenomenon, fecal pellets were collected from mice who were injected with PBS control or with EVs from KPC, PSC and co-culture conditions two weeks after education. The microbiome was analyzed and we observed significant changes in the α and β-diversity profiles within two weeks. Each of the experimental conditions induced changes in the microbial flora. Compared to the PBS control injections, EVs from stellate cells, specifically induce changes in the populations of bacteria from the family coriobacteriaceae, genus Adlercreutzia. While, EVs from the cancer cells modulate levels of bacteria from the phylum Tenericutes, family Mogibacteriaceae, genus Adlercreutzia. There was a significant enrichment of bacteria fro the phylum Firmicutes, genus coprococcus, when mice were educated with EVs from the co-culture educated samples These findings provide ample evidence for the potent bioactivity of EVs to induce changes in the murine microbiome.

The most important finding in our study is the very local effect in the stroma. In both mouse and human tissue, the stroma adjacent to the tumor showed high expression of the protein while in adjacent normal tissue, though acinii show elevated levels of the protein, the surrounding tissues however, do not show expression of these biomarkers. Earlier studies have shown that there are different populations of fibroblasts within the stroma indicative of the heterogeneity [71–74]. Perhaps, these distinct subpopulations of cells respond differently to the secretion of proteins in the immediate vicinity. Additional studies are needed to characterize these stromal differences in pancreatic cancer. Thus, we propose that there are distinct cell populations in the immediate TME that are modulated when EVs are secreted from cancer cells in both the primary and metastatic site allowing for selective gene regulation. Additionally, since we see the expression of proteins except Mmp3 in very early stages of the KPC pancreatic cancer development, one could hypothsize that these factors could profuce a local effect first and distant effect later. However, our studies indicate that both Kif5b and Sfrp2 seem to be good robust candidates for early detection of pancreatic cancer.

The major limitation of the immunohistochemical approch is the availability of effective single antibodies that are reactive to both the mouse and human tissues. In our study, most markers that were selected for validation were discarded as they were mono species reactive. This situation can be easily remedied by using other non-antibody based strategies such as using nanobodies, DARPins, monobodies or affibodies or MALDI-based visualization techniques. Overall, the goal of our study was to identify early cancer-stromal specific changes in our study system and identify the biomarker that would be useful in identifying these early stage interactions between cancer cells- TME for PDAC detection. We have provides a novel mechanistic insight into the ways by which the EVs potentiate changes in the gut microbiome in our mice studies thereby shifting the microbiome towards a more ‘cancerous’ phenotype.

5. Conclusions

In summary, our research provides a framework for identifying early EV biomarkers in pancreatic cancer using a multi-omics approach. Early EV education in mice can induce changes in the microbiome that could later influence metastases. Rapid analysis of protein candidates from the EVome assayed on mouse-human hybrid TMAs helped in identifying the potentially novel role of Kif5b and Sfrp2 as promising protein candidate biomarkers for the detection of early onset of pancreatic cancer. Lastly, our study, also provides evidence for the the role of the EVome in directly influencing and modulating the gut microbiome in murine models of PDAC.

Abbreviations

1. **EV**: Extracellular vesicles
2. **TME**: Tumor Microenvironment
3. **EVome**: Extravessicular Proteome
4. **EVtrap**: Extracellular vesicles total recovery and purification
5. **MMP**: Matrix Mettaloprotease
6. **PDAC**: Pancreatic Ductal Adenocarcinoma
7. **KPC**: KrasG12D/p53R172H/Pdx1Cre mouse pancreatic cancer GEMM model
8. **PSC**: Pancreatic Stellat Cell
9. **DMEM**: Dulbecco's Modified Eagles Medium
10. **FBS**: Fetal Bovine Serum
11. **CoC**: Co-culture
12. **EMT**: Epithelial Mesenchymal Transition
13. **GEMM**: Genetically Engineered Mouse Model
14. **ECM**: Extracellular Matrix

Declarations

Author Contributions:

"Conceptualization, H.K.C.J and A.K.S; methodology, H.K.C.J., R.S., J.L.C.R., T.K., S.L., A.M., B.A.G., A.F., H.A., J.T., A.B.E, W.A.T., A.I., R.D., S.R., and R.S.; software, J.L.C.R., J.T., M.H., W.A.T., and A.I; writing—H.K.C.J., R.S., S.L., J.L.C.R.,T.K., A.M., B.A.G., H.A., and J.T.; visualization, H.K.C.J., J.L.C.R., J.T., and M.A. ;

Animal welfare and Surgeries- S.L., A.M., B.A.G., and A.F.; TMA generation and sample acquisition-A.B.E and M.M.B.; Supervision, H.K.C.J and A.K.S.; pathology and histological analyses, M.G-B.; funding acquisition, A.K.S.. All authors have read and agreed to the published version of the manuscript."

Funding:

This research was funded by the following grants awarded to Dr. Ashok Kumar Saluja from the Florida Department of Health: James Esther King (JEK) 8JK07 and 9JK09, Bankhead Coley Grant 8BC07 and internal funding from the Sylvester Comprehensive Cancer Center (SCCC).

Institutional Review Board Statement:

The study was conducted according to the guidelines of the Declaration of Helsinki and approved by the Institutional Review Board of the Sylvester Comprehensive Cancer Center protocol code 20060858 approved on 6 June 2007.

Data Availability Statement:

All mass spectrometry and sequencing raw files along with analyses files have been deposited at Biostudies under the accession number S-BSST794.

Acknowledgments:

We acknowledge Vania Almeida and the University of Miami Transmission Electron Microscopy Core for assistance with the generation of EM images. We acknowledge Robert Diaz, Aliya Khan and Daniel Bilbao Cortes for help with pathological processing of samples. We thank Dr. Sabita Roy and Dr. Sundaram Ramakrishnan for critical review of the manuscript. I would like to thank Ms. Alexandra Hill for the constant support and consistent guidance in helping get the manuscript to completion.

Conflicts of Interest:

A.K.S. is one of the inventors of Minnelide, which has been licensed to Minneamrita Therapeutics by the University of Minnesota; and is its cofounder and CSO. A.I. and W.A.T. are principals at Tymora Analytical Operations that developed and patented EVtrap. The rest of the authors declare no conflict of interest.

References

1. [https://www.cancer.org/content/dam/cancer-org/research/cancer-facts-and-statistics/annual-cancer-facts-and-figures/2022/2022-cancer-facts-and-figures.pdf]
2. Humphris JL, Chang DK, Johns AL, Scarlett CJ, Pajic M, Jones MD, Colvin EK, Nagrial A, Chin VT, Chantrill LA*et al*: **The prognostic and predictive value of serum CA19.9 in pancreatic cancer**. *Ann Oncol*2012, **23**(7):1713-1722.

3. Azizian A, Ruhlmann F, Krause T, Bernhardt M, Jo P, Konig A, Kleiss M, Leha A, Ghadimi M, Gaedcke J: **CA19-9 for detecting recurrence of pancreatic cancer**. *Sci Rep*2020, **10**(1):1332.
4. Goonetilleke KS, Siriwardena AK: **Systematic review of carbohydrate antigen (CA 19-9) as a biochemical marker in the diagnosis of pancreatic cancer**. *Eur J Surg Oncol*2007, **33**(3):266-270.
5. Park J, Choi Y, Namkung J, Yi SG, Kim H, Yu J, Kim Y, Kwon MS, Kwon W, Oh DY*et al*: **Diagnostic performance enhancement of pancreatic cancer using proteomic multimarker panel**. *Oncotarget*2017, **8**(54):93117-93130.
6. Mellby LD, Nyberg AP, Johansen JS, Wingren C, Nordestgaard BG, Bojesen SE, Mitchell BL, Sheppard BC, Sears RC, Borrebaeck CAK: **Serum Biomarker Signature-Based Liquid Biopsy for Diagnosis of Early-Stage Pancreatic Cancer**. *J Clin Oncol*2018, **36**(28):2887-2894.
7. Kim H, Kang KN, Shin YS, Byun Y, Han Y, Kwon W, Kim CW, Jang JY: **Biomarker Panel for the Diagnosis of Pancreatic Ductal Adenocarcinoma**. *Cancers (Basel)*2020, **12**(6).
8. Diamandis EP: **The failure of protein cancer biomarkers to reach the clinic: why, and what can be done to address the problem?** *BMC Med*2012, **10**:87.
9. Ruivo CF, Bastos N, Adem B, Batista I, Duraes C, Melo CA, Castaldo SA, Campos-Laborie F, Moutinho-Ribeiro P, Morao B*et al*: **Extracellular Vesicles from Pancreatic Cancer Stem Cells Lead an Intratumor Communication Network (EVNet) to fuel tumour progression**. *Gut*2022.
10. Zhao Y, Zheng Y, Zhu Y, Zhang Y, Zhu H, Liu T: **M1 Macrophage-Derived Exosomes Loaded with Gemcitabine and Deferasirox against Chemoresistant Pancreatic Cancer**. *Pharmaceutics*2021, **13**(9).
11. Liu H, Qiao S, Fan X, Gu Y, Zhang Y, Huang S: **Role of exosomes in pancreatic cancer**. *Oncol Lett*2021, **21**(4):298.
12. Mees ST, Mardin WA, Wendel C, Baeumer N, Willscher E, Senninger N, Schleicher C, Colombo-Benkmann M, Haier J: **EP300–a miRNA-regulated metastasis suppressor gene in ductal adenocarcinomas of the pancreas**. *Int J Cancer*2010, **126**(1):114-124.
13. Li Z, Tao Y, Wang X, Jiang P, Li J, Peng M, Zhang X, Chen K, Liu H, Zhen P*et al*: **Tumor-Secreted Exosomal miR-222 Promotes Tumor Progression via Regulating P27 Expression and Re-Localization in Pancreatic Cancer**. *Cell Physiol Biochem*2018, **51**(2):610-629.
14. Wang S, Ji J, Song J, Li X, Han S, Lian W, Cao C, Zhang X, Li M: **MicroRNA-182 promotes pancreatic cancer cell proliferation and migration by targeting beta-TrCP2**. *Acta Biochim Biophys Sin (Shanghai)*2016, **48**(12):1085-1093.
15. Kosaka N: **Decoding the Secret of Cancer by Means of Extracellular Vesicles**. *J Clin Med*2016, **5**(2).
16. Truong LH, Pauklin S: **Pancreatic Cancer Microenvironment and Cellular Composition: Current Understandings and Therapeutic Approaches**. *Cancers (Basel)*2021, **13**(19).
17. Provenzano PP, Cuevas C, Chang AE, Goel VK, Von Hoff DD, Hingorani SR: **Enzymatic targeting of the stroma ablates physical barriers to treatment of pancreatic ductal adenocarcinoma**. *Cancer Cell*2012, **21**(3):418-429.

18. Apte MV, Haber PS, Darby SJ, Rodgers SC, McCaughan GW, Korsten MA, Pirola RC, Wilson JS: **Pancreatic stellate cells are activated by proinflammatory cytokines: implications for pancreatic fibrogenesis**. *Gut*1999, **44**(4):534-541.
19. Vonlaufen A, Joshi S, Qu C, Phillips PA, Xu Z, Parker NR, Toi CS, Pirola RC, Wilson JS, Goldstein D*et al*: **Pancreatic stellate cells: partners in crime with pancreatic cancer cells**. *Cancer Res*2008, **68**(7):2085-2093.
20. Whatcott CJ, Diep CH, Jiang P, Watanabe A, LoBello J, Sima C, Hostetter G, Shepard HM, Von Hoff DD, Han H: **Desmoplasia in Primary Tumors and Metastatic Lesions of Pancreatic Cancer**. *Clin Cancer Res*2015, **21**(15):3561-3568.
21. Wang X, Luo G, Zhang K, Cao J, Huang C, Jiang T, Liu B, Su L, Qiu Z: **Hypoxic Tumor-Derived Exosomal miR-301a Mediates M2 Macrophage Polarization via PTEN/PI3Kgamma to Promote Pancreatic Cancer Metastasis**. *Cancer Res*2018, **78**(16):4586-4598.
22. Charles Jacob HK, Charles Richard JL, Signorelli R, Kashuv T, Lavania S, Vaish U, Boopathy R, Middleton A, Boone MM, Sundaram R*et al*: **Modulation of Early Neutrophil Granulation: The Circulating Tumor Cell-Extravesicular Connection in Pancreatic Ductal Adenocarcinoma**. *Cancers (Basel)*2021, **13**(11).
23. Ayres Pereira M, Chio IIC: **Metastasis in Pancreatic Ductal Adenocarcinoma: Current Standing and Methodologies**. *Genes (Basel)*2019, **11**(1).
24. Costa-Silva B, Aiello NM, Ocean AJ, Singh S, Zhang H, Thakur BK, Becker A, Hoshino A, Mark MT, Molina H*et al*: **Pancreatic cancer exosomes initiate pre-metastatic niche formation in the liver**. *Nat Cell Biol*2015, **17**(6):816-826.
25. Zhang W, Zhang K, Zhang P, Zheng J, Min C, Li X: **Research Progress of Pancreas-Related Microorganisms and Pancreatic Cancer**. *Front Oncol*2020, **10**:604531.
26. Kuracha MR, Thomas P, Tobi M, McVicker BL: **Role of cell-free network communication in alcohol-associated disorders and liver metastasis**. *World J Gastroenterol*2021, **27**(41):7080-7099.
27. Garcia-Etxebarria K, Clos-Garcia M, Telleria O, Nafria B, Alonso C, Iruarrizaga-Lejarreta M, Franke A, Crespo A, Iglesias A, Cubiella J*et al*: **Interplay between Genome, Metabolome and Microbiome in Colorectal Cancer**. *Cancers (Basel)*2021, **13**(24).
28. Pothula SP, Xu Z, Goldstein D, Biankin AV, Pirola RC, Wilson JS, Apte MV: **Hepatocyte growth factor inhibition: a novel therapeutic approach in pancreatic cancer**. *Br J Cancer*2016, **114**(3):269-280.
29. Wu X, Li L, Iliuk A, Tao WA: **Highly Efficient Phosphoproteome Capture and Analysis from Urinary Extracellular Vesicles**. *J Proteome Res*2018, **17**(9):3308-3316.
30. Yu Z, Zhao S, Ren L, Wang L, Chen Z, Hoffman RM, Zhou J: **Pancreatic cancer-derived exosomes promote tumor metastasis and liver pre-metastatic niche formation**. *Oncotarget*2017, **8**(38):63461-63483.
31. Cox J, Mann M: **MaxQuant enables high peptide identification rates, individualized p.p.b.-range mass accuracies and proteome-wide protein quantification**. *Nat Biotechnol*2008, **26**(12):1367-1372.

32. Cox J, Neuhauser N, Michalski A, Scheltema RA, Olsen JV, Mann M: **Andromeda: a peptide search engine integrated into the MaxQuant environment**. *J Proteome Res*2011, **10**(4):1794-1805.
33. Eden E, Navon R, Steinfeld I, Lipson D, Yakhini Z: **GOrilla: a tool for discovery and visualization of enriched GO terms in ranked gene lists**. *BMC Bioinformatics*2009, **10**:48.
34. Fabregat A, Jupe S, Matthews L, Sidiropoulos K, Gillespie M, Garapati P, Haw R, Jassal B, Korninger F, May B*et al*: **The Reactome Pathway Knowledgebase**. *Nucleic Acids Res*2018, **46**(D1):D649-D655.
35. Gohl DM, Vangay P, Garbe J, MacLean A, Hauge A, Becker A, Gould TJ, Clayton JB, Johnson TJ, Hunter R*et al*: **Systematic improvement of amplicon marker gene methods for increased accuracy in microbiome studies**. *Nat Biotechnol*2016, **34**(9):942-949.
36. Bolyen E, Rideout JR, Dillon MR, Bokulich NA, Abnet CC, Al-Ghalith GA, Alexander H, Alm EJ, Arumugam M, Asnicar F*et al*: **Reproducible, interactive, scalable and extensible microbiome data science using QIIME 2**. *Nat Biotechnol*2019, **37**(8):852-857.
37. Chong J, Liu P, Zhou G, Xia J: **Using MicrobiomeAnalyst for comprehensive statistical, functional, and meta-analysis of microbiome data**. *Nat Protoc*2020, **15**(3):799-821.
38. Hingorani SR, Wang L, Multani AS, Combs C, Deramaudt TB, Hruban RH, Rustgi AK, Chang S, Tuveson DA: **Trp53R172H and KrasG12D cooperate to promote chromosomal instability and widely metastatic pancreatic ductal adenocarcinoma in mice**. *Cancer Cell*2005, **7**(5):469-483.
39. Vonlaufen A, Phillips PA, Yang L, Xu Z, Fiala-Beer E, Zhang X, Pirola RC, Wilson JS, Apte MV: **Isolation of quiescent human pancreatic stellate cells: a promising in vitro tool for studies of human pancreatic stellate cell biology**. *Pancreatology*2010, **10**(4):434-443.
40. Andreu Z, Yanez-Mo M: **Tetraspanins in extracellular vesicle formation and function**. *Front Immunol*2014, **5**:442.
41. Hoshino A, Kim HS, Bojmar L, Gyan KE, Cioffi M, Hernandez J, Zambirinis CP, Rodrigues G, Molina H, Heissel S*et al*: **Extracellular Vesicle and Particle Biomarkers Define Multiple Human Cancers**. *Cell*2020, **182**(4):1044-1061 e1018.
42. Lau C, Kim Y, Chia D, Spielmann N, Eibl G, Elashoff D, Wei F, Lin YL, Moro A, Grogan T*et al*: **Role of pancreatic cancer-derived exosomes in salivary biomarker development**. *J Biol Chem*2013, **288**(37):26888-26897.
43. Puente A, Fortea JI, Cabezas J, Arias Loste MT, Iruzubieta P, Llerena S, Huelin P, Fabrega E, Crespo J: **LOXL2-A New Target in Antifibrogenic Therapy?** *Int J Mol Sci*2019, **20**(7).
44. Simpson RJ, Kalra H, Mathivanan S: **ExoCarta as a resource for exosomal research**. *J Extracell Vesicles*2012, **1**.
45. Keshava Prasad TS, Goel R, Kandasamy K, Keerthikumar S, Kumar S, Mathivanan S, Telikicherla D, Raju R, Shafreen B, Venugopal A*et al*: **Human Protein Reference Database–2009 update**. *Nucleic Acids Res*2009, **37**(Database issue):D767-772.
46. Tijeras-Raballand A, Hilmi M, Astorgues-Xerri L, Nicolle R, Bieche I, Neuzillet C: **Microbiome and pancreatic ductal adenocarcinoma**. *Clin Res Hepatol Gastroenterol*2021, **45**(2):101589.

47. Mima K, Nakagawa S, Sawayama H, Ishimoto T, Imai K, Iwatsuki M, Hashimoto D, Baba Y, Yamashita YI, Yoshida N*et al*: **The microbiome and hepatobiliary-pancreatic cancers**. *Cancer Lett*2017, **402**:9-15.
48. Li JJ, Zhu M, Kashyap PC, Chia N, Tran NH, McWilliams RR, Bekaii-Saab TS, Ma WW: **The role of microbiome in pancreatic cancer**. *Cancer Metastasis Rev*2021, **40**(3):777-789.
49. Chakladar J, Kuo SZ, Castaneda G, Li WT, Gnanasekar A, Yu MA, Chang EY, Wang XQ, Ongkeko WM: **The Pancreatic Microbiome is Associated with Carcinogenesis and Worse Prognosis in Males and Smokers**. *Cancers (Basel)*2020, **12**(9).
50. Wen B, Xu LY, Li EM: **LOXL2 in cancer: regulation, downstream effectors and novel roles**. *Biochim Biophys Acta Rev Cancer*2020, **1874**(2):188435.
51. Kim IK, Lee YS, Kim HS, Dong SM, Park JS, Yoon DS: **Specific protein 1(SP1) regulates the epithelial-mesenchymal transition via lysyl oxidase-like 2(LOXL2) in pancreatic ductal adenocarcinoma**. *Sci Rep*2019, **9**(1):5933.
52. Wang C, Xu S, Tian Y, Ju A, Hou Q, Liu J, Fu Y, Luo Y: **Lysyl Oxidase-Like Protein 2 Promotes Tumor Lymphangiogenesis and Lymph Node Metastasis in Breast Cancer**. *Neoplasia*2019, **21**(4):413-427.
53. Shao B, Zhao X, Liu T, Zhang Y, Sun R, Dong X, Liu F, Zhao N, Zhang D, Wu L*et al*: **LOXL2 promotes vasculogenic mimicry and tumour aggressiveness in hepatocellular carcinoma**. *J Cell Mol Med*2019, **23**(2):1363-1374.
54. Barker HE, Bird D, Lang G, Erler JT: **Tumor-secreted LOXL2 activates fibroblasts through FAK signaling**. *Mol Cancer Res*2013, **11**(11):1425-1436.
55. Torres S, Garcia-Palmero I, Herrera M, Bartolome RA, Pena C, Fernandez-Acenero MJ, Padilla G, Pelaez-Garcia A, Lopez-Lucendo M, Rodriguez-Merlo R*et al*: **LOXL2 Is Highly Expressed in Cancer-Associated Fibroblasts and Associates to Poor Colon Cancer Survival**. *Clin Cancer Res*2015, **21**(21):4892-4902.
56. Tian J, Sun HX, Li YC, Jiang L, Zhang SL, Hao Q: **LOXL 2 Promotes The Epithelial-Mesenchymal Transition And Malignant Progression Of Cervical Cancer**. *Onco Targets Ther*2019, **12**:8947-8954.
57. Hong X, Yu JJ: **Silencing of lysyl oxidaselike 2 inhibits the migration, invasion and epithelialtomesenchymal transition of renal cell carcinoma cells through the Src/FAK signaling pathway**. *Int J Oncol*2019, **54**(5):1676-1690.
58. Moon HJ, Finney J, Xu L, Moore D, Welch DR, Mure M: **MCF-7 cells expressing nuclear associated lysyl oxidase-like 2 (LOXL2) exhibit an epithelial-to-mesenchymal transition (EMT) phenotype and are highly invasive in vitro**. *J Biol Chem*2013, **288**(42):30000-30008.
59. Cuevas EP, Eraso P, Mazon MJ, Santos V, Moreno-Bueno G, Cano A, Portillo F: **LOXL2 drives epithelial-mesenchymal transition via activation of IRE1-XBP1 signalling pathway**. *Sci Rep*2017, **7**:44988.
60. Peinado H, Del Carmen Iglesias-de la Cruz M, Olmeda D, Csiszar K, Fong KS, Vega S, Nieto MA, Cano A, Portillo F: **A molecular role for lysyl oxidase-like 2 enzyme in snail regulation and tumor progression**. *EMBO J*2005, **24**(19):3446-3458.
61. Minici C, Rigamonti E, Lanzillotta M, Monno A, Rovati L, Maehara T, Kaneko N, Deshpande V, Protti MP, De Monte L*et al*: **B lymphocytes contribute to stromal reaction in pancreatic ductal**

adenocarcinoma. *Oncoimmunology*2020, **9**(1):1794359.

62. de Jong OG, van Balkom BW, Gremmels H, Verhaar MC: **Exosomes from hypoxic endothelial cells have increased collagen crosslinking activity through up-regulation of lysyl oxidase-like 2**. *J Cell Mol Med*2016, **20**(2):342-350.
63. Gobin E, Bagwell K, Wagner J, Mysona D, Sandirasegarane S, Smith N, Bai S, Sharma A, Schleifer R, She JX: **A pan-cancer perspective of matrix metalloproteases (MMP) gene expression profile and their diagnostic/prognostic potential**. *BMC Cancer*2019, **19**(1):581.
64. Holmberg C, Ghesquiere B, Impens F, Gevaert K, Kumar JD, Cash N, Kandola S, Hegyi P, Wang TC, Dockray GJ*et al*: **Mapping proteolytic processing in the secretome of gastric cancer-associated myofibroblasts reveals activation of MMP-1, MMP-2, and MMP-3**. *J Proteome Res*2013, **12**(7):3413-3422.
65. Kaur A, Webster MR, Marchbank K, Behera R, Ndoye A, Kugel CH, 3rd, Dang VM, Appleton J, O'Connell MP, Cheng P*et al*: **sFRP2 in the aged microenvironment drives melanoma metastasis and therapy resistance**. *Nature*2016, **532**(7598):250-254.
66. Henriksen SD, Madsen PH, Larsen AC, Johansen MB, Drewes AM, Pedersen IS, Krarup H, Thorlacius-Ussing O: **Cell-free DNA promoter hypermethylation in plasma as a diagnostic marker for pancreatic adenocarcinoma**. *Clin Epigenetics*2016, **8**:117.
67. Bu XM, Zhao CH, Zhang N, Gao F, Lin S, Dai XW: **Hypermethylation and aberrant expression of secreted frizzled-related protein genes in pancreatic cancer**. *World J Gastroenterol*2008, **14**(21):3421-3424.
68. Tanaka Y, Kanai Y, Okada Y, Nonaka S, Takeda S, Harada A, Hirokawa N: **Targeted disruption of mouse conventional kinesin heavy chain, kif5B, results in abnormal perinuclear clustering of mitochondria**. *Cell*1998, **93**(7):1147-1158.
69. Nakata T, Hirokawa N: **Point mutation of adenosine triphosphate-binding motif generated rigor kinesin that selectively blocks anterograde lysosome membrane transport**. *J Cell Biol*1995, **131**(4):1039-1053.
70. Zhao L, Liu H, Luo S, Moorman PG, Walsh KM, Li W, Wei Q: **Associations between genetic variants of KIF5B, FMN1, and MGAT3 in the cadherin pathway and pancreatic cancer risk**. *Cancer Med*2020, **9**(24):9620-9631.
71. Dominguez CX, Muller S, Keerthivasan S, Koeppen H, Hung J, Gierke S, Breart B, Foreman O, Bainbridge TW, Castiglioni A*et al*: **Single-Cell RNA Sequencing Reveals Stromal Evolution into LRRC15(+) Myofibroblasts as a Determinant of Patient Response to Cancer Immunotherapy**. *Cancer Discov*2020, **10**(2):232-253.
72. Wang Y, Liang Y, Xu H, Zhang X, Mao T, Cui J, Yao J, Wang Y, Jiao F, Xiao X*et al*: **Single-cell analysis of pancreatic ductal adenocarcinoma identifies a novel fibroblast subtype associated with poor prognosis but better immunotherapy response**. *Cell Discov*2021, **7**(1):36.
73. Sebastian A, Hum NR, Martin KA, Gilmore SF, Peran I, Byers SW, Wheeler EK, Coleman MA, Loots GG: **Single-Cell Transcriptomic Analysis of Tumor-Derived Fibroblasts and Normal Tissue-Resident**

Fibroblasts Reveals Fibroblast Heterogeneity in Breast Cancer. *Cancers (Basel)*2020, **12**(5).

74. Chen K, Wang Q, Li M, Guo H, Liu W, Wang F, Tian X, Yang Y: **Single-cell RNA-seq reveals dynamic change in tumor microenvironment during pancreatic ductal adenocarcinoma malignant progression**. *EBioMedicine*2021, **66**:103315.

Figures

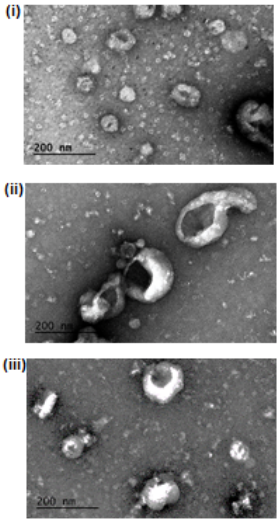

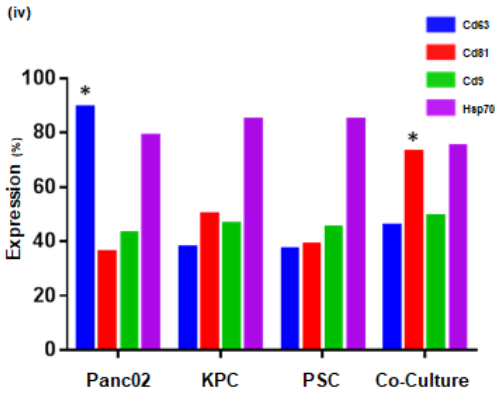

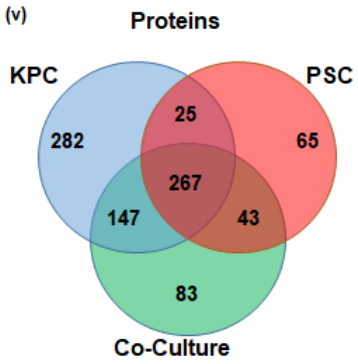

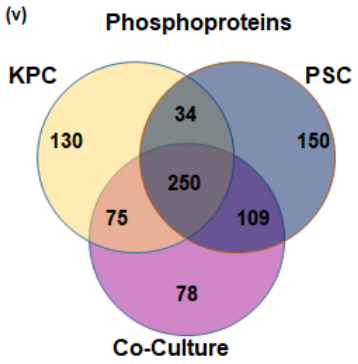

Reactome analysis

Figure 1

Transmission electron microscopy of EVs isolated from (i) KPC Cells, (ii) PSC Cells and (iii) EVs isolated from KPC and PSC co-culture conditions. All magnifications are shown at 300000X while the scale bar is at 200 nm. (iv) Flow cytometric characterization of Cd63, Cd81, Cd9 EV surface biomarkers and Hsp70 protein in PancO2 cell line and EVs isolated from KPC, PSC and Co-culture conditions. Distribution of overlap of proteins and phosphoprotein identifications from the KPC, PSC and CoC conditions. Distribution is represented as a Venn diagram of (v) proteins and (vi) phosphoproteins.

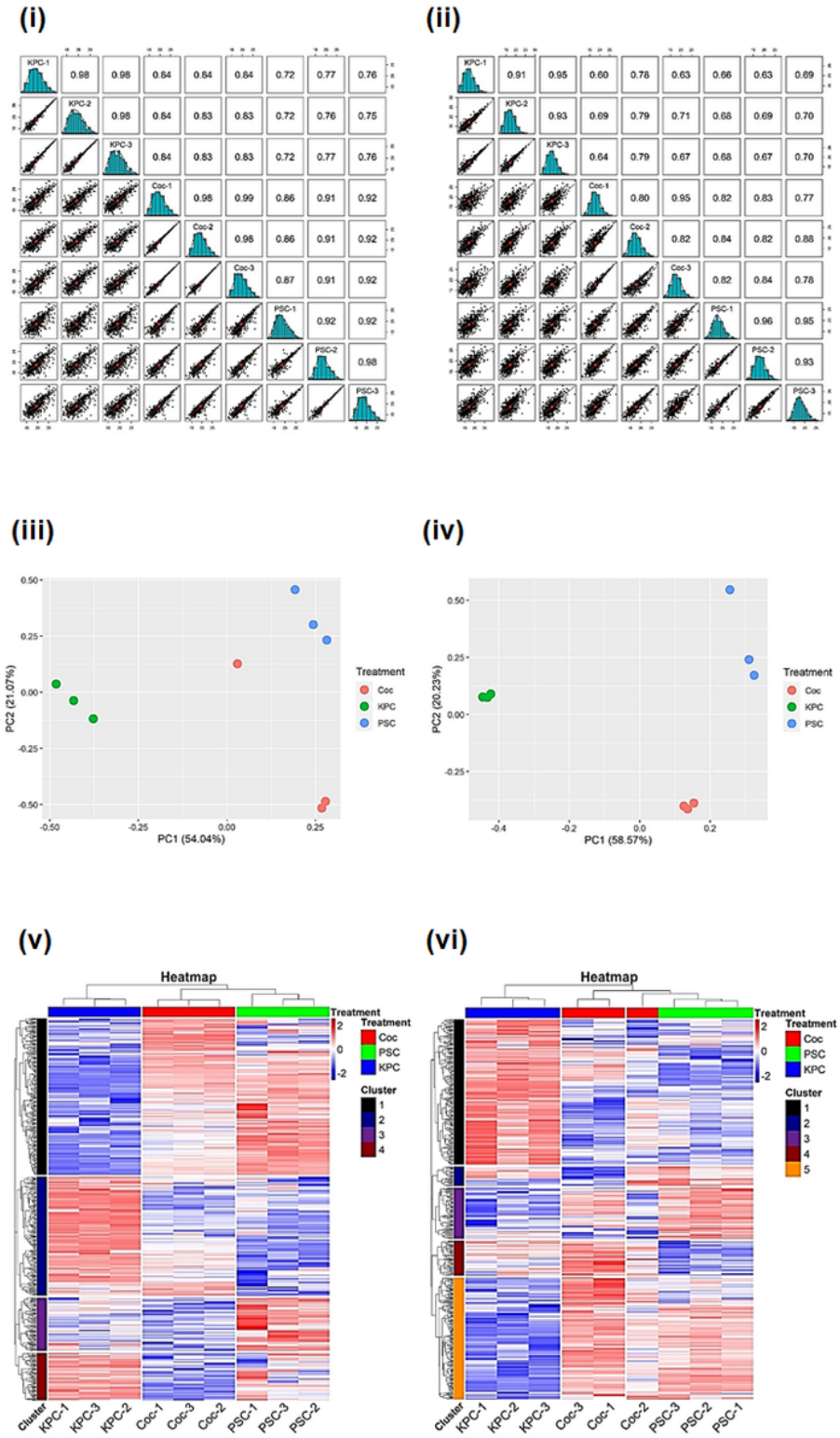

Figure 2

Multiscatter plots of (i) proteins and (ii) phosphoproteins identified from mass spectrometric analyses of the EVome representing correlation between data points obtained from the different experimental groups and biological triplicates among the KPC, PSC and CoC (Co-Culture) conditions. Principal component analyses plot of the (iii) proteins and (iv) phosphoproteins identified to show similarity between samples. Unsupervised hierarchical clustering of (v) proteins and (vi) phosphoproteins identified by mass

spectrometry in the triplicate samples of EVs analyzed by mass spectrometry. Distribution of protein expression patterns is classified into clusters with proteins showing similar behavior clustering together.

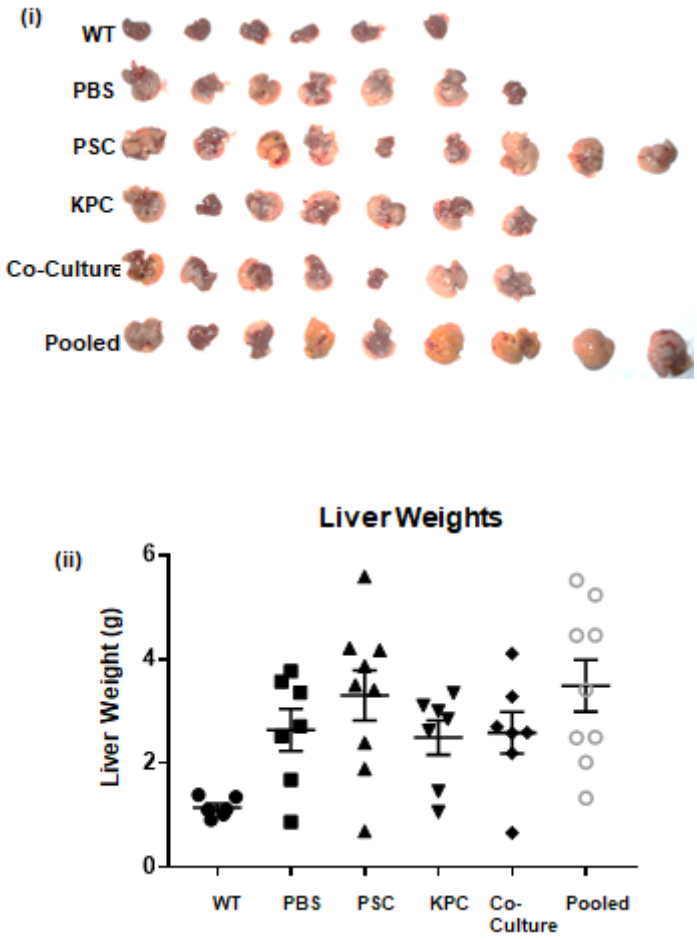

Figure 3

(i) Liver sizes in different groups after 21 days post implantation. (ii) Plot of liver weights in each group with X-axis showing the groups and Y-axis representing liver weights in grams.

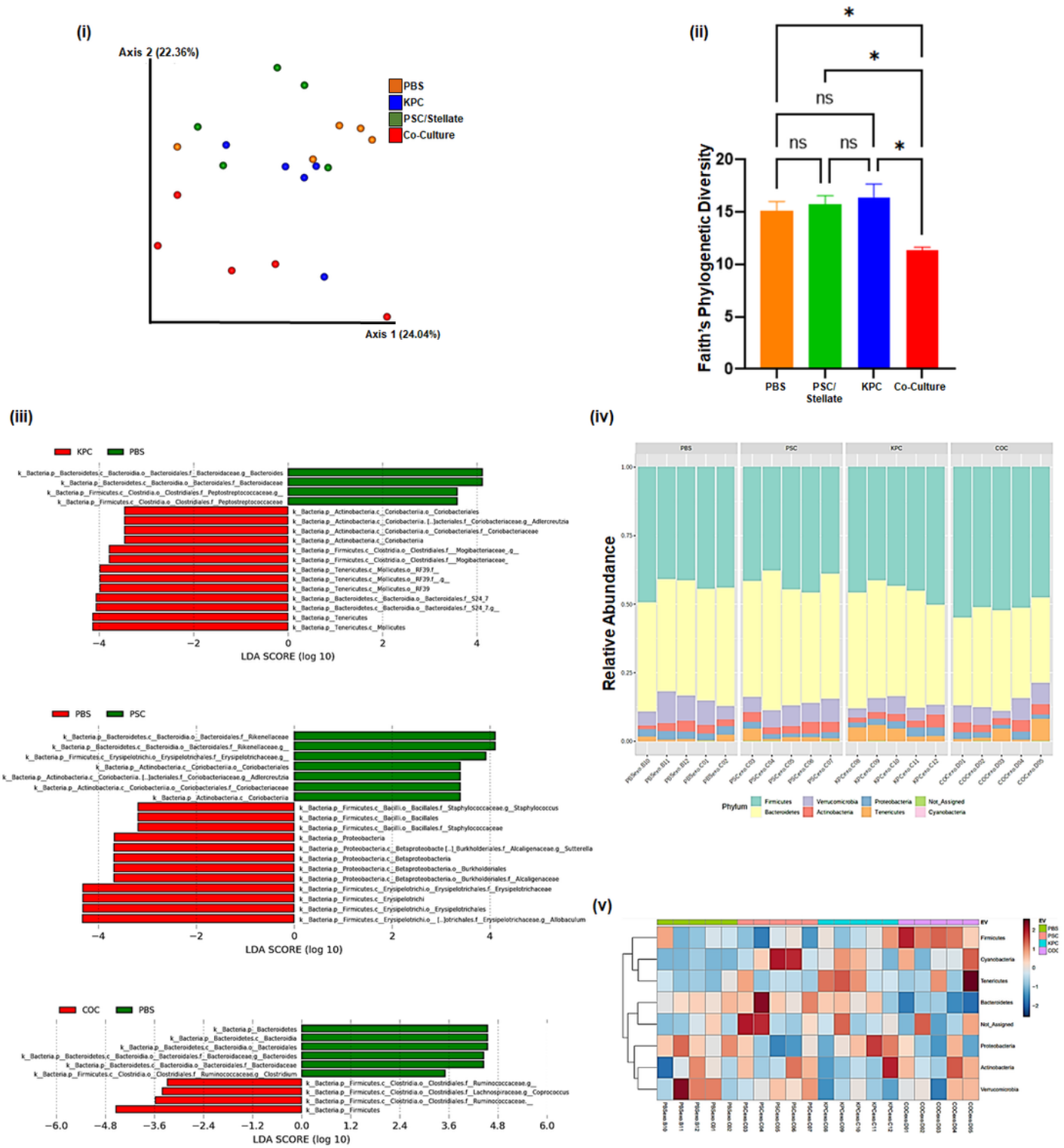

Figure 4

(i) Principal coordinate analysis (PCA) plot of weighted UniFrac distances (metric of β diversity) with q<0.01 among all four groups (ii) Faith's phylogenetic diversity (metric of α diversity) at sequencing depth of 19200; * represents p<0.05; ns represents not significant (iii) LefSe (Linear Discriminant Analysis Effect Size) analysis of bacterial samples among samples KPC Vs PBS control, PSC Vs PBS Control, and CoC (Co-culture) Vs PBS control. The top discriminative bacterial taxa identified between the represented

conditions is shown. (iv) Phylum level bacterial composition in the different experimental conditions. Samples include PBS, KPC, CoC and PSC conditions. N= 5 samples were considered for the analysis. (v) Heatmap of OTU abundance at the phylum level.

Figure 5

Representative cores of mouse and human normal and diseased pancreas from the hybrid TMA. The same sections across different TMAs are shown stained for histomorphological stain. Masson's Trichrome, followed by staining for protein marker Kif5b, Sfrp2, Loxl2, and Mmp3. All imaged are at a magnification of 2.68X.

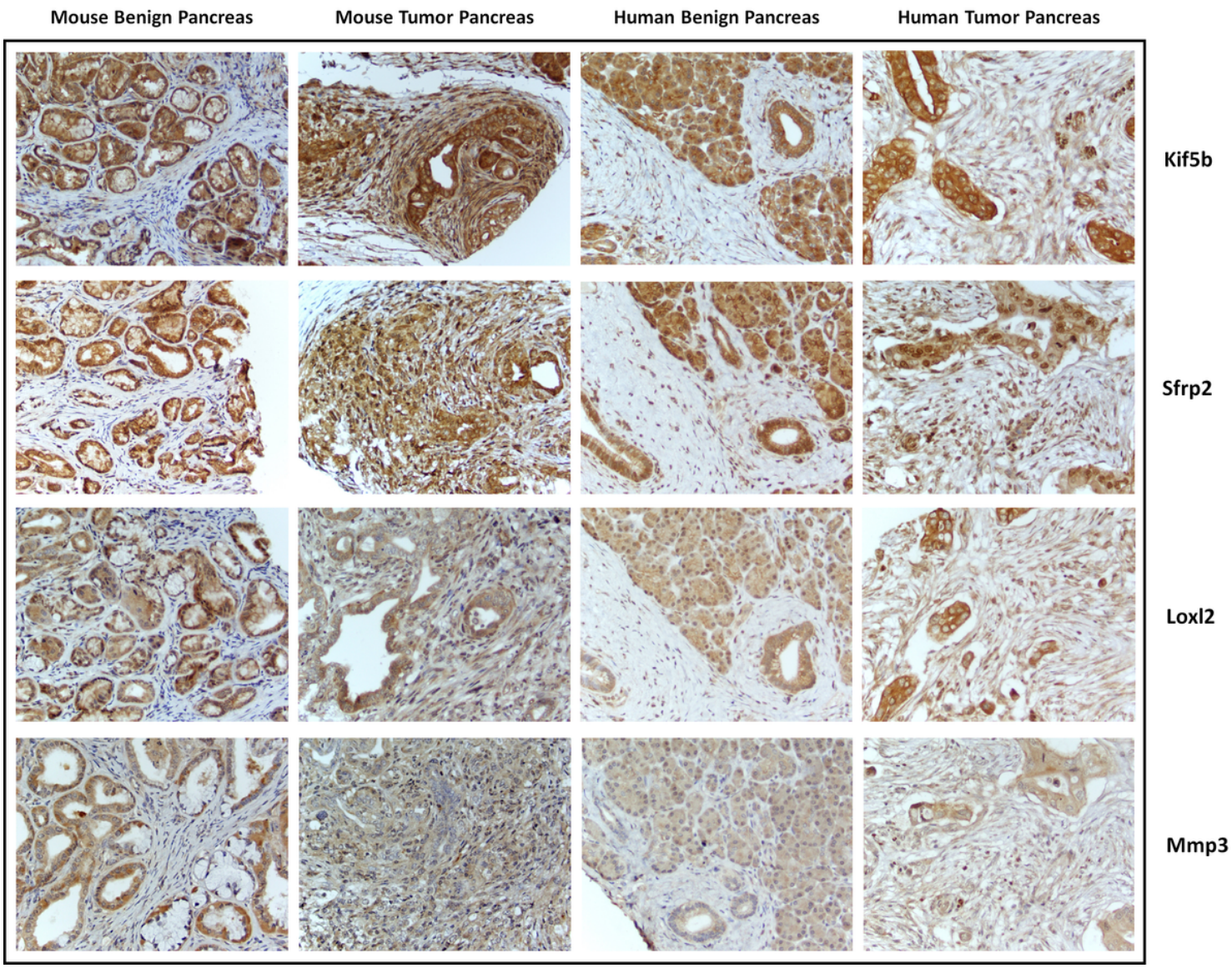

Figure 6

Representative images of mouse and human benign and tumor pancreas at 40X magnification. Stained for Kif55, Sfrp2, Loxl2, and Mmp3. Differential expression of the proteins in stroma and tumor are assessed.

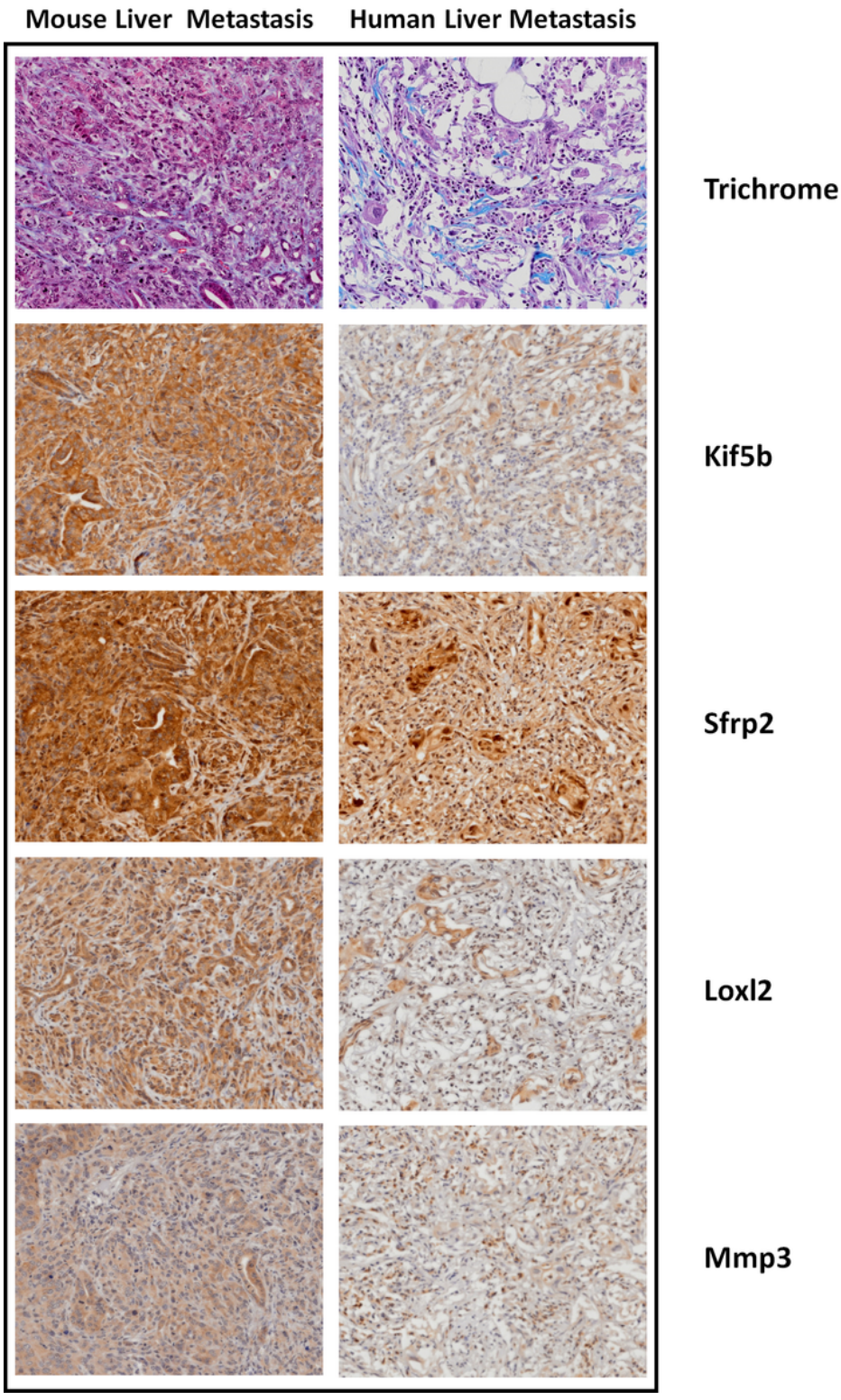

Figure 7

Assessment of biomarker staining in distant liver metastases in mouse and human tumor samples. Histological control Masson's Trichrome stain and histological staining for markers validated in this study: Kif5b, Sfrp2, Loxl2, and Mmp3. Image magnifications are at 20X.

Supplementary Files

This is a list of supplementary files associated with this preprint. Click to download.

- SupplementaryFileS1.xlsx
- SupplementaryFileS2.xlsx
- SupplementaryFileS3.pdf
- SupplementaryFileS4.xlsx
- SupplementaryFileS5.xlsx
- SupplementaryFileS6.xlsx
- SupplementaryFigure1.pptx
- SupplementaryFigure2.pptx
- SupplementaryFigure3.pptx
- SupplementaryFigure4.pptx